Geosciences and Engineering, Vol. 13, No. 2 (2025), pp. 105–126.
https://doi.org/10.33030/geosciences.2025.02.008

HEAVY MINERAL SAND FROM THE VICINITY OF TIBOLDDARÓC, BÜKKALJA REGION, NE HUNGARY

CSILLA BALASSA[1*], NORBERT NÉMETH[2], FERENC KRISTÁLY[3], FERENC MÓRICZ[4], DÉLIA BULÁTKÓ-DEBUS[5]
[1,2,3,4,5]*Institute of Exploration Geosciences, University of Miskolc*
[1*]*csilla.balassa@uni-miskolc.hu*
[2]*norbert.nemeth1@uni-miskolc.hu*
[3]*ferenc.kristaly@uni-miskolc.hu*
[4]*ferenc.moricz@uni-miskolc.hu*
[5]*delia.bulatko-debus@uni-miskolc.hu*
[1]*https://orcid.org/0000-0001-6134-5262*
[2]*https://orcid.org/0000-0002-4264-5136*
[3]*https://orcid.org/0000-0002-0075-5994*
[4]*https://orcid.org/0000-0001-6708-3507*

Abstract: Recent placer deposits of ilmenite-rich heavy sand were found in the Bükkalja region, in the vicinity of Tibolddaróc, sampled in a stream bed and in a rill on a dirt road. These placers consist mostly of plagioclase feldspars, quartz and ilmenite. In this paper, the composition of the sampled placer is studied, as well as the composition of some neighboring Miocene ignimbrite and tuff samples, potential source rocks of heavy minerals. The amount of ilmenite can reach 20-30 wt% in the bulk sample, but it is almost 50 wt% in the 0.212 – 0.3 mm grain size fraction. With simple magnetic separation, this enrichment can be increased to 70 wt%. In addition to ilmenite, heavy sand contains a relatively high amount of allanite and zircon as well.

***Keywords**: Ilmenite, allanite, placer deposit, ignimbrite, tuff, Bükkalja*

1. INTRODUCTION

The ilmenite is a usual accessory both in igneous and metamorphic rocks and a common constituent of placer deposits, due to its high specific gravity (4.72). In addition to rutile, it is the main source of Ti, whose metallic form is a critical element in the European Union (Bowles et al., 2011). Most of the ilmenite is mined from placer deposits, but there are also hard rock deposits (ultramafic to mafic layered intrusions or anorthosite massifs) (Murphy and Frick, 2006). The most significant ilmenite placer deposits are marine, situated in coastal areas, like in India, Bangladesh, Brazil, Australia, New Zealand, South Africa, Egypt (Angusamy et al., 2005; MacDonald and Rozendaal, 1995; Nayak et al., 2012; Prates Hallal et al., 2025; Rahman et al., 2020; Ramakrishnan et al., 1997; Roy, 1999; Wassef, 1981; Wells and Haverkamp, 2020), but for example in Virginia alluvial deposits occur (Herz et al., 1970). Less significant ilmenite placer deposits are situated even in

European countries, such as Ukraine and in Greenland (eluvial, alluvial and marine placers as well) (Ganzha et al., 2023; Kolb et al., 2016). Non-formula element content in ilmenite is often a useful indicator of the provenance area, especially the Mn/Mg ratio and the Ni, Cr, V, Co concentration (Bhattacharyya et al., 1997). The Ti/(Ti + Fe) ratio in ilmenites refers to the degree of alteration, due to Fe removal from the structure in the presence of water, in acidic environment. Leached ilmenite then alters to pseudorutile, finally to leucoxene (Mücke and Bhadra Chaudhuri, 1991).

Ilmenite is known as a common accessory mineral in certain Miocene volcanic rocks of the Bükkalja region (e. g. Czuppon et al., 2012; Harangi et al., 2005; Lukács et al., 2022). Small-scale ilmenite-rich placers were found in the region, near Tibolddaróc, as a proximal weathering product of the volcanic formations redeposited by runoffs. In addition to ilmenite, the sands have a small enrichment of allanite and zircon as well. Although the extension of these recent heavy mineral accumulations detectable on the surface is far smaller than the economic placers, probably it is the indication of bigger alluvial deposits in the sole of the valleys. This study introduces the composition of a sampled deposit in the stream bed of the temporary runoff Száraz-tó-ér, with a comparison of the heavy mineral content of the potential source rock types and a local recent natural concentrate. The current state of research does not aim to investigate the extent and economic significance of a potential resource, only to indicate its existence.

2. GEOLOGICAL SETTING

The Bükkalja region is an extensive outcrop area of Miocene volcanics in NE Hungary. The magmatism responsible for its generation was the result of the subduction of Vardar / Magura microplate under the ALCAPA microplate, which also carried volatiles (Kovács and Szabó, 2008). Due to the rotation of the microplates, lithospheric thinning occurred (Csontos et al., 1992). The Bükkalja region is characterized by silicic ignimbrite units, supplemented with fall-out deposits and paleosols (Biró et al., 2020). Originally, three silicic horizons were identified with various tools, including K-Ar geochronology and paleomagnetic studies: the Lower, the Middle, and Upper Rhyolitic Tuff Complexes (Szakács et al., 1998). Newer, mainly zircon trace element chemistry and U/Pb dating-based studies indicate eight eruption phases (Lukács et al., 2018), based on which the Miocene volcanic sequence was divided into four lapilli tuff formations, namely Tihamér Rhyolite Lapilli Tuff (18.2–17.1 Ma), Bogács Dacite Lapilli Tuff (16.8–16.2 Ma), Tar Dacite Lapilli Tuff (15.1–14.8 Ma) and Harsány Rhyolite Lapilli Tuff (14.7–14.4 Ma) Formations (Lukács et al., 2022). In another division, Hencz et al. (2024) identified a single formation with eleven lithological members and fourteen eruption events, mainly based on lithostratigraphic and geochemical signatures. Although the general composition of the rocks is silicic, in the case of the Bogács Tuff Formation primitive basic melts also had a role in the volcanism (Czuppon et al., 2012).

3. MATERIALS AND METHODS

3.1 Sample preparation and analytical methods

Collected rock samples were first crushed in a steel mortar up to 1 mm, then pulverized in porcelain and agate mortar up to 65 and 5 μm, respectively. Before grinding, ilmenite sand samples were first homogenized and rinsed with distilled water to remove the clay fraction. After that, the remaining heavy mineral fraction was dried and sieved with the following mesh sizes: 2 mm, 1 mm, 500 μm, 300 μm, 212 μm and 106 μm. From an ilmenite-rich fraction, the ilmenite was further enriched with a magnet. From the sample, TD-5K clay and heavy mineral separation was made with the application of gravitational settling in distilled water.

Thin sections and polished sections were embedded into two-component resin (Araldit, 2020), and after three days drying, they were polished with silicium carbide abrasive powder and paper. Thin sections were stuck on glass plates, and thinned to 30 μm, while polished sections were also polished with diamond-bearing abrasive gel. For chemical analyses of the samples, the 65 μm powder was used. Analyses were done by wavelength-dispersive X-ray fluorescence spectrometry (WD-XRF), with a Rigaku Supermini 200 WDXRF instrument (200W Pd X-ray tube, 50 kV accelerating voltage, 4 mA current, LiF200 / PET / XR25 crystals, 4 g pellets with CEREOX) to determine the concentration of major and minor elements, as well as some trace elements (e.g. Zr). Trace element concentrations of five samples (four ignimbrite and a tuff) were analyzed by the laboratory of ALS with ICP-MS (ME-MS81 analyses, based on Li-borate digestion and four acid dissolution), on the same powder, then XRF.

The mineralogical composition was determined by X-ray powder diffraction (XRD) on the 5 μm powders. For the measurement, a Bruker D8 Advance (40 kV, 40 mA Cu K-α radiation) instrument was used with a Vantec-1 position-sensitive detector, in parallel beam geometry using a Göbel mirror. The phase identification was carried out using DiffracPlus EVA software, based on the ICDD PDF2 2005 database, while the quantitative evaluation in Topas4 software with Rietveld refinement method (NIST SRM 640b Si calibration standard, crystal structure information from AMCSD (Downs and Hall-Wallace, 2003)).

Electron microprobe studies on the carbon-coated polished slabs were used to measure the chemical composition of individual grains (energy dispersive X-ray spectrometry, EDX point measurements and X-ray element maps) and to observe the distribution of the different minerals on back-scattered electron (BSE) images. For the electron microprobe studies, a SamX-controlled JEOL JXA 8600 Superprobe was used (20 kV accelerator voltage, 20 nA beam current), equipped with an SDD-EDX detector.

Textural characteristics and mineralogy were investigated also by optical microscopy on the thin sections in transmitted light (Zeiss Imager A2m AXIO polarization microscope, Zeiss AxioCam MRc5 camera). The flowchart of the research process is shown in Figure 1.

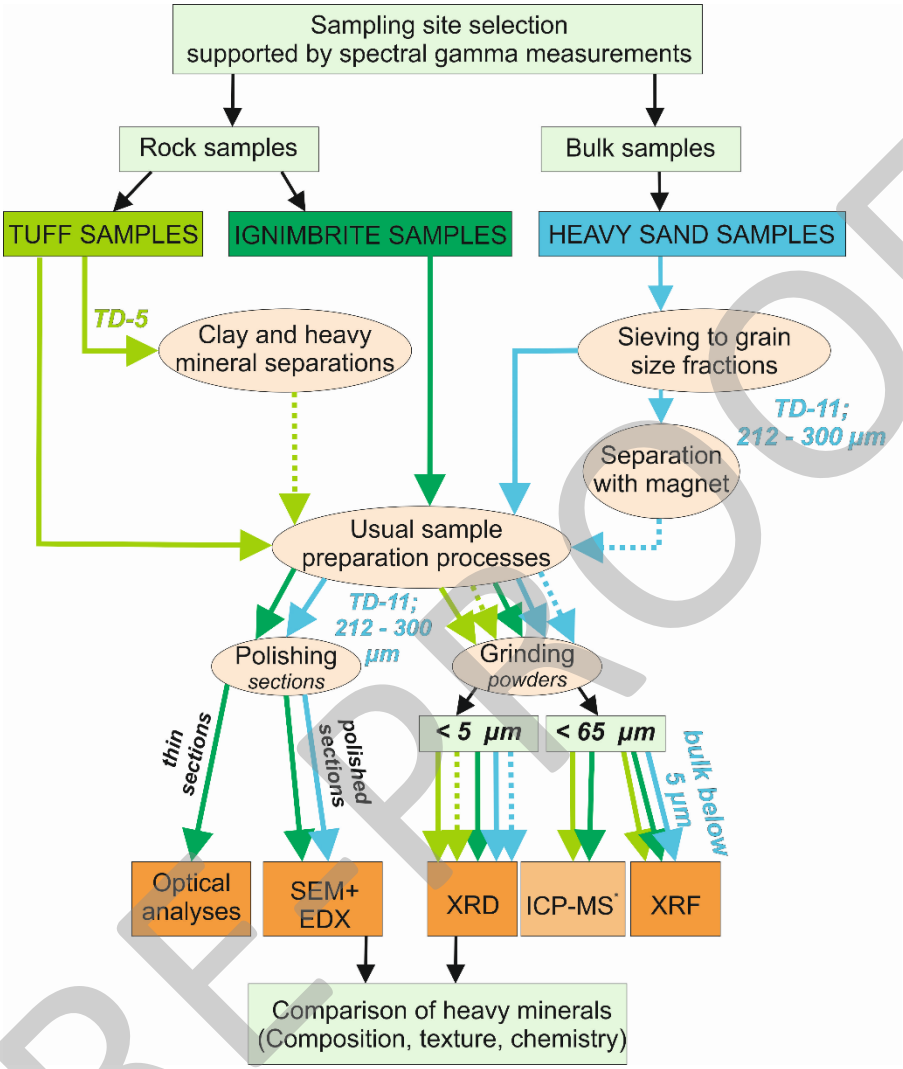

Figure 1

*Flowchart of the research process. *Analytical methods, except ICP-MS were performed in the Institute of Exploration Geosciences, University of Miskolc*

3.2 Samples and sampling methods

Sampling was supported by natural gamma measurement (Gamma Surveyor portable scintillation detector). Sites of sampling and spectral gamma measurements are shown in Figure 2. Integral measurements indicate relatively homogenous gamma activity within the investigated area but higher activity over the sampled placer. At certain points, including sampled exposures spectral gamma analysis was performed. The K values in the territory are usually between 2-5 wt%, the equivalent Th (eTh) values 15-20 ppm, while the maximum value of the equivalent U (eU) is

around 8 ppm (Table 1). The stream bed with the heavy mineral accumulation stands out by high eTh value. Samples TD-2 and TD-3 are massive ignimbrites from the Bér-oldal quarry, from the vicinity of Tibolddaróc. (From measuring point TD-K-1 no sample was collected.) Both samples are welded and have a fiamme-bearing structure, but while the matrix of TD-2 is yellowish, TD-3 is pinkish. Sample TD-4 is taken from a nearby gully. It is very similar to the other two samples, as it is also a fiamme-bearing ignimbrite of brownish color. Samples TD-5A, 5K and 5F are pumice-rich lapilli tuff samples representing the lower (A), middle (K) and upper (F) bed groups of a ravine wall of the Száraz-tó-ér stream. The material is relatively loose, the most compact is the middle part. Sample TD-7 is a pumice-rich tuff, collected near Kőhodály, a historical artificial sheepfold carved into the cliff. Sample TD-10 is ilmenite-rich heavy sand collected from the depression of a dirt road. Sample TD-9 is a grey ignimbrite collected from debris in the vicinity of the TD-10. In the case of TD-9 and TD-10 spectral gamma data were not recorded, because the small volume of the sampled material is suppressed by the effect of the background. Sample TD-11 is heavy sand, from the bed of the Száraz-tó-ér stream. This sample showed the highest eTh-content in the area with 30 ppm eTh. A more in-depth test series would be required to determine the stratigraphic position with complete certainty, but the observed textural, chemical and mineralogical features and topographic situation of the outcrops suggest in case of most of the samples that the most likely candidate is the Bogács Dacite Lapilli Tuff Formation. This formation is increasingly mafic from bottom to top. The sampled tuffs probably belong to the Harsány Lapilli Tuff Formation, which was also described from the vicinity of Tibolddaróc. These two formations were described to contain zircon, apatite, ilmenite and allanite as accessories (Babinszki et al., 2024; Lukács et al., 2022).

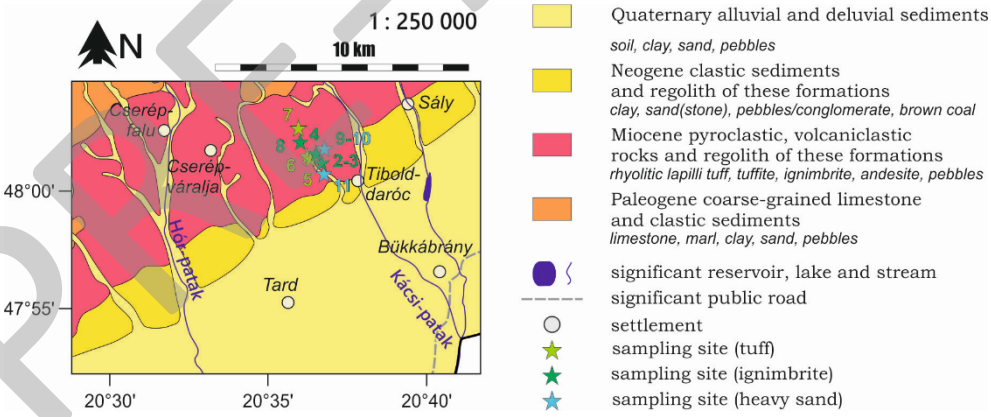

Figure 2

Schematic geological map of the surroundings of Tibolddaróc by marking the sampling sites with their number.

Table 1

Location of the sampling sites and results of the spectral gamma ray measurements in the vicinity of Tibolddaróc

	EOV Y	EOV X	K [wt%]	eU [ppm]	eTh [ppm]	Dose rate[nGy/h]	comment
TD-1	767065	288400	3.93	3.4	19.45	119.55	Welded ignimbrite, quarry *(samples TD-2 and TD-3)*
TD-2	767035	288420	3.60	5.5	19.3	126.7	
TD-3			3.52	3.15	17.65	108.5	
TD-4	766835	288755	3.50	4.05	19.5	117.85	Welded ignimbrite, gully *(sample TD-4)*
TD-5A	766615	288545	4.87	5.5	19.35	143.35	Lapilli tuff, ravine *(samples TD-5A, TD-5K, TD-5F)*
TD-5K	766615	288545	4.01	7.9	19.65	146.6	
TD-5F	766615	288545	4.58	4.8	19.9	137.15	
TD-5b	766615	288545	3.68	5.9	19.9	131.65	
TD-6	766500	288650	4.25	6.45	18.35	138.35	Bomb-rich lapilli tuff, ravine *(no sample)*
TD-7	766145	289765	3.89	5.7	15.8	123.2	Lapilli tuff (Kőhodály) *(sample TD-7)*
TD-8	766220	289220	2.96	4.45	15.05	102.1	Welded ignimbrite *(no sample)*
TD-9	767170	288955	Gamma spectrum not measured				Welded ignimbrite *(sample TD-9)*
TD-10							Heavy sand *(sample TD-10)*
TD-11	767155	287960	2.19	5.15	29.6	131.9	Heavy sand in stream bed *(sample TD-11)*

3.3 Grain size distribution of heavy sand samples

Heavy sand samples were sieved into grain size fractions before any other sample preparation processes were made. The total weights of the samples before the sieving were about 150 g and 175 g, in the case of samples TD-10 and TD-11, respectively. As the fractions above 2 mm are partly composed of artificial material (brick and glass fragments) and lithoclasts, they were ignored during further analyses. Total sample weights excluding this fraction were 131 and 102 g, respectively. The grain size distributions are smooth enough in the case of both samples, but not the same (Figure 3). The dominant size fractions in sample TD-10 are the 212 – 300 μm and 300 – 500 μm, while in the case of sample TD-11 the 300 – 500 μm and 500 μm – 1

mm fractions. The 0 – 106 µm fraction is insignificant in both samples (1.6 and 0.65 wt%).

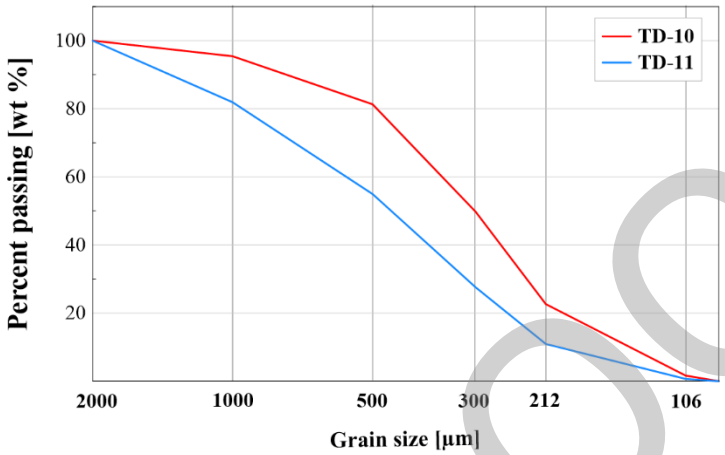

Figure 3

Grain-size distribution of samples TD-10 and TD-11

4. RESULTS

4.1 Chemical composition

Major, minor and trace element concentrations of the studied samples measured by XRF are summarized in Tables 2 and 3. Major element concentrations of the ignimbrite and tuff samples are similar: about 70 wt% SiO_2, 14 wt% Al_2O_3, 0,5-0,6 MgO, 1-3 wt% CaO and Na_2O, 3-5 wt% K_2O and 2-3 wt% Fe_2O_3. This composition corresponds to the rhyolitic - dacitic fields in the TAS diagram (Figure 4a). The exception is sample TD-9, with its lower SiO_2 and K_2O and higher CaO and Fe_2O_3 concentrations (basaltic andesite composition). The REE+Y content of the samples studied (TD-2, TD-3, TD-9, TD-7) is between 180 and 310 ppm (Table 4) light REEs are more enriched than heavy ones. Negative Eu anomaly is characteristic. Zr concentration is between 180 – 300 ppm, Th between 9 -19 ppm, Nb 11 - 14 ppm, TiO_2 0.1 – 1 %. The Zr and TiO_2 contents are generally higher in the ignimbrite samples examined than in tuff samples, but for other HFSEs the data is insufficient to establish such relationships. Trace element concentrations also indicate rhyolitic-dacitic composition in the Winchester-Floyd diagram (Figure 4b), except in the case of sample TD-9. The upper crust normalized (Rudnick and Gao, 2013) trace element plot and chondrite normalized (Anders and Grevesse, 1989) REE plots are shown in Figure 5. It is important to highlight that all indicated concentration data refer to the whole rock compositions, not for volcanic glass.

Table 2

Major and minor element concentrations of the analyzed samples based on XRF measurement.
**bulk sample below 300 μm*

Sample	SiO_2	Al_2O_3	MgO	CaO	Na_2O	K_2O	Fe_2O_3	MnO	TiO_2	P_2O_5	S	TOTAL
	%											
TD-7	72.4	13.7	0.61	2.16	1.89	3.87	2.14	0.036	0.276	0.045	0.01	97.1
TD-2	67.7	14.1	0.63	2.32	2.82	3.31	2.91	0.020	0.406	0.068	0.01	94.3
TD-3	68.8	14.1	0.66	2.41	2.74	3.35	3.00	0.040	0.321	0.055	0.01	95.6
TD-4	66.1	14.2	0.54	2.94	2.80	3.22	3.60	0.023	0.427	0.082	0.02	94.0
TD-5 A	73.1	13.0	0.52	1.03	1.10	4.52	2.07	0.058	0.236	0.010	0.02	95.7
TD-5 F	73.3	13.1	0.51	0.98	1.06	4.35	1.91	0.053	0.216	0.009	0.01	95.5
TD-5 K	69.9	13.8	0.93	1.15	0.85	3.90	3.03	0.076	0.267	0.013	0.02	94.0
TD-9	56.8	16.5	1.63	5.41	1.83	1.73	7.33	0.073	1.091	0.175	0.01	92.5
TD-10*	26.3	5.5	1.74	1.98	0.94	0.63	23.7	0.319	**32**	0.171	0.02	93.3
TD-11*	27.5	5.6	1.25	1.65	0.96	0.69	20.5	0.305	**36**	0.095	0.02	94.5

Table 3

Trace element concentrations of the analyzed samples based on XRF measurement. F and As are always below detection limit (<0.3 and <10 ppm, respectively).
**bulk sample below 300 μm*

Sample	Cu	Zn	Pb	Rb	Sr	Ba	Cr	Co	Ni	Zr
	ppm									
TD-7	22	59	21	169	306	1080	23	<10	20	172
TD-2	20	53	17	126	222	932	25	<10	17	254
TD-3	20	56	19	154	230	998	25	<10	18	230
TD-4	13	54	19	130	247	1017	25	<10	17	299
TD-5 A	17	175	30	283	136	1218	17	<10	21	164
TD-5 F	20	61	24	283	127	1151	18	<10	18	161
TD-5 K	19	68	18	254	134	1106	19	<10	24	168
TD-9	23	77	45	57	264	521	65	16	22	226
TD-10*	<10	108	<10	<10	39	1893	294	39	25	417
TD-11*	<10	80	<10	<10	36	2072	204	36	21	437

Table 4

Concentration values of some selected trace elements, based on ICP-MS

Sample	Ba	Cr	Nb	Rb	Sn	Sr	Ta	Th	U	V	∑REE+Y
TD-3	1030	20	13.6	119	3	223	1.6	18.05	4	45	279.34
TD-2	909	21	13.6	108	2.5	190.5	1.1	19.25	3.48	51	312.97
TD-4	995	18	13.45	115	2.7	219	1.1	17.15	3.8	44	272.64
TD-9	505	71	14.2	60.2	18.3	292	1	8.76	2.31	196	183.56
TD-7	1070	13	11.25	141.5	3.6	250	1	17.6	4.34	29	182.35

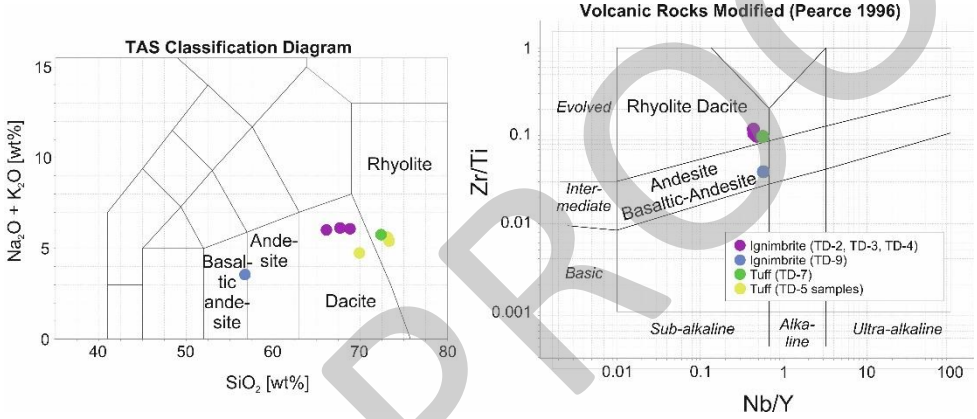

(a) (b)

Figure 4

Rock classification plots for the studied samples. (a) TAS diagram, (b) Winchester-Floyd diagram.

From samples TD-10 and TD-11 XRF analyses were performed only on the <300 µm fractions. Based on it, about 35-40 wt% of the samples are composed of TiO_2, with approximately 20 wt% Fe_2O_3, 30 wt% SiO_2 and 5 wt% Al_2O_3. MnO (~0,1 wt%) and Cr (60-70 ppm) are also enriched in these samples, compared to the upper crust. TiO_2 values in TD-10 and TD-11 are not reliable, as the XRF instrument is not calibrated to such high values. Most of the trace elements have not been measured yet.

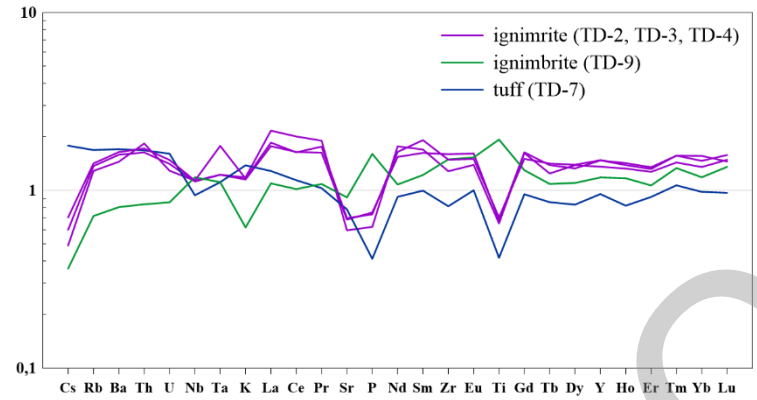

(a)

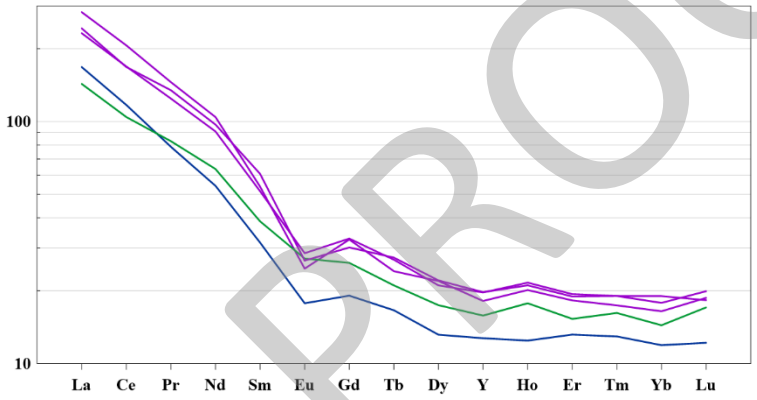

(b)

Figure 5

Upper crust normalized trace element (a) and chondrite normalized REE concentrations(b) of some selected samples

4.2 XRD analysis of the heavy sand samples

All six sample fractions were separately pulverized for XRD analyses for both samples. Mineral constituents are the same in every fraction (ilmenite, hematite, zircon, allanite, apatite, quartz, cristobalite, plagioclase feldspars, sanidine, pyroxenes), but their ratios vary (Table 5). Mineral composition of the complete samples below 1 mm was not measured but calculated using the weights and the mineral compositions of the individual fractions. Based on that, the total ilmenite content in the samples (excluding materials over 2 mm) is around 30 wt% (sample TD 10) and 20 wt% (sample TD 11), with significant feldspar (almost 30 wt%) and quartz (10-20 wt%) content Based on the XRD results, the most characteristic plagioclase feldspar is the labradorite in both samples. As for the individual factions, the highest ilmenite concentration is present in the 106 – 212 µm fraction and 212 – 300 µm fractions (35-45 wt%), but generally the concentration of the ilmenite is above 20 wt% in every fraction below 500 µm. Compared to these fractions, the ones

above 500 mm are relatively poor in ilmenite, but they have a high ratio of quartz, cristobalite and feldspars. Zircon is usually low, but it can reach almost 4 wt% in the finest fractions of the samples.

Table 5

Mineralogical composition of each fraction of the heavy mineral sand samples (in wt%, based on XRD; nd: not detected)

	TD-10						TD-11					
upper mesh size [µm]	**2000**	**1000**	**500**	**300**	**212**	**106**	**2000**	**1000**	**500**	**300**	**212**	**106**
Quartz	25.37	28.07	9.95	5.90	7.04	15.84	28.08	33.88	14.80	9.02	11.87	24.21
Cristo-balite low	13.04	8.18	2.06	1.43	1.08	0.70	11.27	5.94	1.82	1.52	1.27	0.53
Anorthite	1.89	1.08	1.00	0.95	1.80	1.64	1.08	0.83	0.81	0.63	1.18	0.64
Andesine	5.50	1.85	0.23	0.11	0.17	13.13	6.36	6.79	0.55	0.35	1.32	7.29
Oligo-clase	14.01	10.74	2.30	1.91	1.82	4.50	15.95	10.14	1.78	1.36	2.12	5.83
Labra-dorite	0.90	11.46	18.54	15.26	17.45	5.20	1.98	8.00	17.75	16.42	19.01	4.60
Sanidine	17.93	11.39	3.16	2.33	0.61	2.18	14.75	8.48	3.55	1.73	2.31	1.53
Biotite 1M	0.39	0.63	0.13	0.48	0.00	0.00	0.50	0.70	0.07	0.06	0.00	0.00
Enstatite	1.12	5.64	10.05	10.22	7.55	5.51	0.84	8.68	11.39	5.37	3.53	5.02
Augite	0.14	0.48	1.74	1.36	1.37	0.77	0.12	0.42	1.37	1.20	0.48	1.54
Ilmenite-(Mg)	0.17	8.78	30.50	37.86	35.45	23.17	0.05	3.37	29.76	45.10	39.71	25.35
Rutile	0.01	0.01	2.11	2.96	3.26	nd	nd	nd	1.27	2.32	2.27	nd
Hematite	1.03	2.08	4.63	6.62	6.40	5.72	0.29	0.42	2.11	4.36	3.65	3.37
Magnetite	1.03	1.00	3.09	3.61	3.99	0.09	0.40	0.36	0.57	0.27	0.52	0.09
Allanite-(Ce)	1.75	1.03	1.79	1.37	1.44	3.13	2.06	1.05	0.87	0.99	0.85	0.72
Zircon	0.69	0.70	0.53	0.37	0.47	3.66	0.80	0.45	0.46	0.69	0.59	3.88
Amor-phous	15.04	6.88	8.19	7.26	10.10	14.86	15.46	10.50	11.07	8.61	9.31	15.50

Based on the concentration data and the grain size distribution, we could calculate the distribution of the various minerals within different fractions (assuming that the total amount of each mineral is 100%). About 30-40 wt% of the ilmenite is in the fractions 212-300 µm and 300-500 µm, while 20-25 in the 0.106-0.212 fractions (Figure 6).

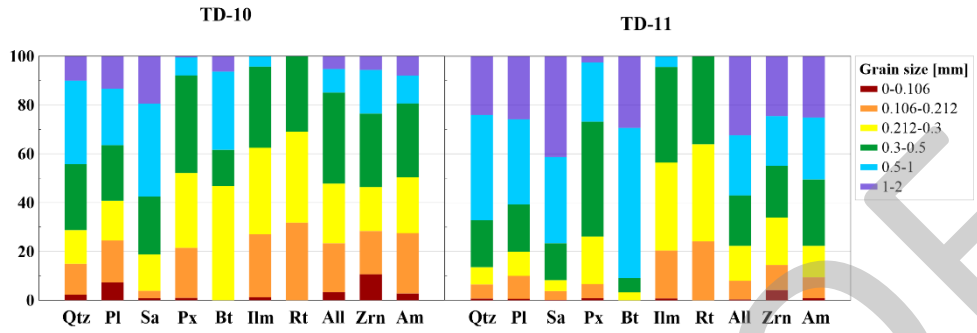

Figure 6

Distribution of some minerals between the different grain size fractions in the heavy sand samples (Qtz = quartz, Pl = plagioclase, Sa = sanidine, Px = pyroxene, Bt = biotite, Ilm = ilmenite, Rt = rutile, All = allanite, Zrn = zircon, Am = amorphous)

The 212-300 µm fraction of sample TD-11 was further separated with a magnet. In the magnetic subfraction the ratio of the ilmenite reached almost 70 wt%. Hematite, rutile, magnetite, and pyroxene, as well as allanite are also enriched in this fraction. The non-magnetic fraction is dominated by feldspars and quartz. Figure 7 compares the XRD diffractograms of the magnetic and non-magnetic fractions, while Table 6 summarizes the mineral quantities.

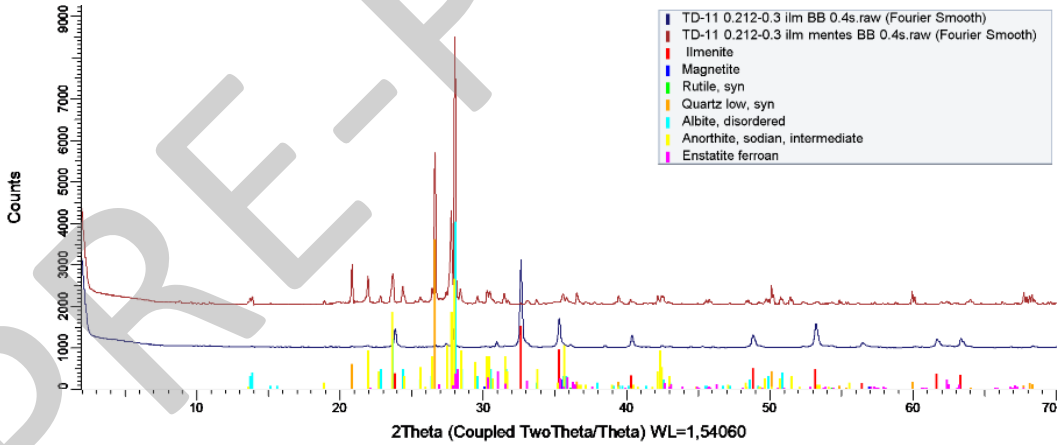

Figure 7

XRD diffractograms of the non-magnetic (red line) and magnetic (dark blue line) fractions of sample TD-11 (grain size between 212 and 300 µm)

Table 6

Mineral composition of the magnetic and non-magnetic fraction of sample TD-11 (grain size between 212 and 300 µm), based on XRD analyses (amorphous is neglected)

	magnetic fraction [wt%]	non-magnetic fraction (wt%)
Quartz	1.69	25.55
Cristobalite low	1.59	2.04
Plagioclase	2.22	58,09
Sanidine Na0.1		6.57
Enstatite	8.76	2.93
Augite Px	4.40	1.02
Ilmenite (Mg)	66.38	
Rutile	3.40	
Hematite	6.81	1.17
Magnetite	1.45	
Allanite-(Ce)	3.18	1.96
Zircon	0.13	0.68

4.3 XRD analysis of rock samples

The rock samples collected from the lapilli tuff and ignimbrite contain mostly the same rock-forming minerals and accessories. Main components are cristobalite, plagioclase feldspars and sanidine, as well as pyroxenes (Table 7). There is no significant difference between samples TD-2, TD-3and TD-4. Quartz content is near zero, and most of the SiO_2 can be identified as cristobalite (5-13 wt%), which is a usual product from the alteration of volcanic glass (Schipper et al., 2020). Plagioclase feldspars constitute about 30 wt%, supplemented with 20% sanidine, pyroxene content is 4-9 wt%. Biotite (1.3-1.7 wt%), as well as smectite (0.6-3 wt %) usually occur in low concentrations. TD-9 is also similar but with lower cristobalite and higher smectite concentration. The amorphous composites of the samples take around 20-40 wt%.

Samples TD-5A, 5K and 5F have high smectite content with a low amount of halloysite and pyrophyllite. The middle part of the section (5K) has the lowest smectite content. Their feldspar association is dominated by plagioclase with a lower amount of sanidine. They do not contain pyroxenes but are extremely rich in amorphous material (almost 80 wt%). Similarly, sample TD-7 lacks pyroxenes, but it also lacks smectites. It does not contain sanidine, but microcline and orthoclase instead.

From TD-5K a gravitational separation experiment was made. The amorphous material is enriched in the coarser fractions, while smectite, halloysite, pyrophyllite, potash feldspars and hematite are in the clay fraction. No ilmenite, zircon or allanite enrichment can be detected in any of the fractions.

Table 7

Mineral composition of the examined samples, based on XRD analysis (in wt%)

	TD-5A	TD-5F	TD-5K	**TD-7**	**TD-2**	**TD-3**	**TD-4**	**TD-9**
Quartz	3.01	2.98	3.48	5.85	0.17	0.89	0.19	0.03
Cristobalite low	2.07	1.38	3.62	1.19	13.07	6.57	10.55	3.37
Anorthite	*1.91*	*2.22*	*2.12*	*0.50*	*2.65*	*3.11*	*1.29*	*2.05*
Labradorite An65	*0.06*	*0.04*	*3.64*	*9.69*	*17.65*	*9.91*	*9.22*	*18.30*
Oligoclase An25	*0.85*	*1.10*	*0.00*	*4.86*	*3.72*	*12.37*	*21.47*	*8.48*
Albite	*3.10*	*2.57*	*1.85*	*0.40*	*5.15*	*0.69*	*4.46*	*3.50*
∑ Plagioclase	**5.93**	**5.93**	**7.61**	**15.44**	**29.17**	**26.08**	**36.46**	**32.32**
Orthoclase				1.55				
Sanidine	3.11	2.86	4.34		19.48	17.39	19.38	20.43
Microcline intermediate				0.69				
Biotite 1M	0.31	0.00	0.28	2.72	1.73	1.33	1.52	0.62
Smectite 15A	5.52	6.50	1.21		2.98	0.65	0.61	5.29
Halloysite 7A	0.04	1.33	0.04					
Pyrophyllite 2M	1.17	1.10	1.68					
Augite				*0.21*	*6.35*	*1.76*	*4.50*	*4.24*
Enstatite				*0.56*	*2.55*	*1.98*	*2.13*	*5.80*
∑ Pyroxene				**0.77**	**8.90**	**3.74**	**6.63**	**10.04**
Ilmenite (Mg)	0.02	0.02	0.03	0.00	0.00	0.00	0.01	0.02
Hematite	0.26	0.53	0.36	0.02	0.03	0.60	0.15	1.48
Zircon				0.03	0.25	0.07	0.31	0.22
Allanite-(Ce)				0.16	0.65	0.01	0.27	0.02
Amorphous	78.56	77.38	77.35	71.57	23.56	42.67	23.93	26.17

4.4 EDX analysis of heavy sand sample

EDX analyses were performed on the 212 - 300 µm fraction of sample TD-11. EDX confirmed that a significant ratio of this fraction consists of ilmenite (Figure 8). The ilmenite grains are generally euhedral to subhedral, angular, or only slightly rounded. Ilmenite contains rare inclusions (apatite, volcanic glass) and intergrowths with other minerals (apatite, feldspars). Chemically it always contains Mg and Mn. The Mn/Mg ratio varies between 0.1 and 0.3, with an outlier value of 0.8. Occasionally V content can also be detected. The Ti/(Ti+Fe) ratio of the ilmenite crystals in atomic percent is generally close to 0.5, meaning that these ilmenites are chemically unaltered. Ilmenite also occurs in the lamellae of a spinel-type Fe- or Fe-Ti-oxide mineral (Ti-bearing magnetite or ulvöspinel). In the opinion of Lattard (1995), in the case of terrestrial rocks, this spinel-ilmenite intergrown texture is most often the result of oxidation processes, which might connect to the reduction of another subsystem of

the same rock. Feldspar minerals are also angular. Measured composition of a few randomly chosen grains corresponds to sanidine, albite, and oligoclase. Subhedral, or slightly rounded allanite-(La) crystals are usual, with about 3 atomic % REE-concentration.

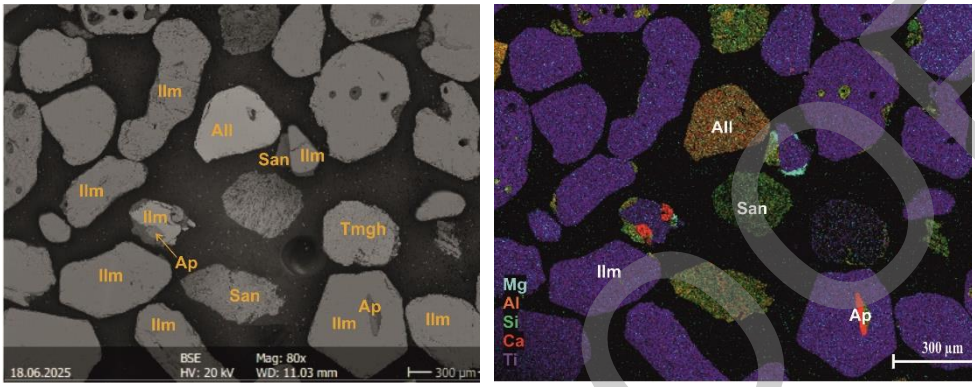

(a) (b)

Figure 8

BSE image (a) and element map (b) of the heavy sand sample, showing the abundant ilmenite grains, with some other characteristic minerals. (All = allanite, Ap = apatite, Ilm = ilmenite, San = sanidine, Tmgh = titanomaghemite?)

4.5 EDX and optical microscopic analysis of ignimbrite samples

Welded ignimbrite samples from the Tibolddaróc quarry and from the neighborhood have fluidal-vitrophyric texture (Figure 9 a-b). The main phenocrysts are sanidine and plagioclase feldspars which are most often euhedral-subhedral, elongated or stocky tables. Oscillation zoning as well as twinning are usual. They can be weathered and fractured. EDX suggests the composition of sanidine, oligoclase, andesine and labradorite. Cristobalite crystals are usually isometric. Biotite is common (except in sample TD-9). They occur as elongated or stocky plates up to several 100 of µm and can be deformed. In most cases, biotite is Fe-dominant and has Ti (1 – 1.4 atomic %), Mn (~0.1 atomic %), V (up to 0.1 atomic %) and Cl (0.1 – 0.3 atomic %) content. In samples TD-4 and TD-2 fiammes are dominated by fibrous, radial clay minerals, but smectite is an ordinary rock-forming mineral in all the other samples. Smectite is Fe-dominant. In sample TD-9 two special compositions can be distinguished: the first one is richer in Mg, Fe and Si, and associated with pyroxene, while the second is Si-rich, and associated with feldspars (Figure 9 c). The composition of smectite from the Tibolddaróc quarry is more homogenous, and intermediate between these two compositions. Pyroxene is especially characteristic of sample TD-9, with a composition corresponding to enstatite. Important accessories in all samples are apatite, zircon, allanite and ilmenite.

Apatite is usually between some 10s of μm and 100 μm. It can be associated with zircon or ilmenite (Figure 9 d). In the first case, it is F-dominant, while in the second case, it is probably OH-dominant (based on F + Cl content lower than stoichiometrically required), although it usually has a low Cl-content as well. Zircon occurs as euhedral to subhedral, usually isometric grains. Its maximum grain size is around 100 μm and occasionally can be detected even with an optical microscope. Allanite from the quarry is partly decomposed along its edge and surrounded by submicrometric monazite crystals (Figure 9 e), which are probably generated from the remobilized REE of the allanite crystals. The chemical composition of the allanite from the quarry differs from the ones from the heavy sand: it is slightly more enriched in REEs, has higher Fe and lower Si and Al concentrations. Ilmenite is usually subhedral. Its size can reach the same 100s of μm. Its Mn/Mg ratio is relatively high (0.5 – 1.4) and sometime have also a small V concentration. Based on the Fe/Ti ratio these ilmenites are also chemically unaltered. In sample TD-9 individual ilmenite crystals are rare, but the presence of intergrown grains with spinel-type Fe-oxides, Fe-Ti-oxides and Ti-oxides with ilmenite is usual. In such kind of composite grains rarely micrometric monazite and cassiterite inclusions can occur (Figure 9 f). Rarely, samples from the quarry also have spinel-type Fe-Ti-oxides, but it is less common. Only one heavy REE-dominant phosphate mineral was detected, in sample TD-9. As the electron beam was able to burn a hole in it, it is possible that this grain was not xenotime-(Y), but its water-bearing variety, churchite-(Y). It should be mentioned that earlier a postvolcanic hydrothermal Sn mineralization was detected in ignimbrite samples from the same quarry as the one sampled for this article (Szakáll and Kristály, 2021).

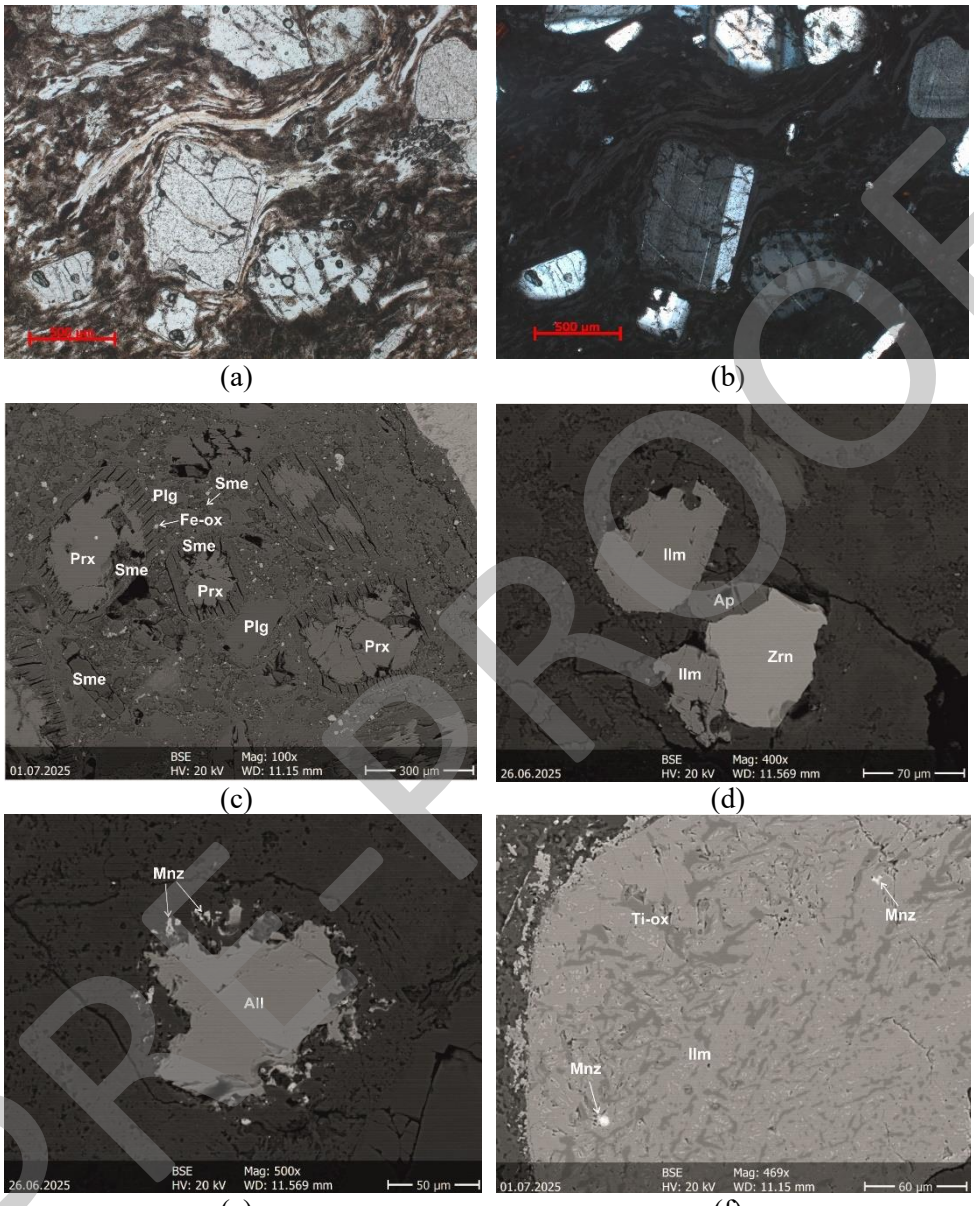

Figure 9

Optical microscopic (a-b) and BSE images of ignimbrite samples (c-f). (a-b): Typical texture of welded ignimbrite from the Tibolddaróc quarry with 1N and XN. (c) Weathered pyroxene and plagioclase crystals (d) Association of ilmenite, apatite and zircon. (e) Allanite with resorbed edges, surrounded by micrometric monazite crystals. (f) Intergrown texture of ilmenite and Ti-oxide, with monazite inclusions. (All = allanite, Ap = apatite, Ilm = ilmenite, Mnz = monazite, Plg = plagioclase, Prx = pyroxene, San = sanidine, Sme = smectite, Zrn = zircon)

5. DISCUSSION AND CONCLUSIONS

The placer deposit studied near Tibolddaróc is enriched in heavy minerals, especially in ilmenite. All heavy minerals of the placer have angular grain shape, and the chemical composition of the ilmenite crystals is pure, without any sign of alteration (Fe/Ti ratio is stoichiometric). Based on these, the provenance territory is in the vicinity of the placer.

The Bükkalja region is characterized by Miocene volcanic formations, with variable erodibility. Generally, welded layers are less prone to being eroded than the unwelded ignimbrites and tuffs. This difference makes the landform of the area so diverse, with elevated plateaus and valleys (Biró et al., 2022). The rock varieties, which are more affected by the physical weathering processes can be the main source of heavy mineral accumulation in the short term. However, in the longer term the welded layers can also serve as a host, as they are more enriched in heavy minerals than tuff layers.

EDX analyses indicate different Mn/Mg ratios for ilmenite crystals from the studied welded ignimbrite samples from Tibolddaróc quarry and from the heavy sand. Similarly, the composition of allanite crystals is also not the same. Another heavy sand sample was collected and studied from the vicinity of Cserépváralja from a stream bed before this study (unpublished results). This sample is not so rich in ilmenite, but it contains similar minerals, again with slightly different composition. For example, allanite from this sample has a higher Fe content and a higher La/Ce ratio than in the ignimbrite from Tibolddaróc quarry.

The above findings indicate that the Miocene volcanic formations of the Bükkalja region in general can be an effective source of heavy mineral accumulation, but heavy mineral crystal chemistry within the Miocene volcanic formations is diverse. Systematic testing of the exact composition of the heavy minerals can be used as a tracer to identify the particular volcanic units and provenance territories of the placer deposits. Although the economic significance of the heavy mineral deposit is currently unknown, the high concentration of ilmenite in the heavy sand samples near Tibolddaróc makes it a potential raw material for future Ti-extraction, if its sufficiently large volume can be confirmed by subsequent research.

ACKNOWLEDGMENTS

The work was supported by the University Research Scholarship Program of the Ministry for Culture and Innovation from the source of the National Research, Development and Innovation Fund. The authors thank the reviewers for their useful suggestions for improving the manuscript.

REFERENCES

Anders, E., Grevesse, N. (1989). Abundances of the elements: Meteoritic and solar. *Geochim Cosmochim Acta* 53, pp. 197–214. https://doi.org/10.1016/0016-7037(89)90286-X

Angusamy, N., Sahayam, J.D., Gandhi, M.S., Rajamanickam, G.V. (2005). Coastal placer deposits of Central Tamil Nadu, India. Marine *Georesources and Geotechnology* 23, pp. 137–174. https://doi.org/10.1080/10641190500192102

Babinszki, E., Piros, O., Csillag, G., Fodor, L., Gyalog, L., Kercsmár, Z., Less, G., Lukács, R., Sebe, K., Selmeczi, I., Szepesi, J., Sztanó, O., Tóth, E. (Eds.), (2024). Lithostratigraphic units of Hungary II. – Cenozoic formations. *Szabályozott Tevékenységek Felügyeleti Hatósága*, Budapest.

Bhattacharyya, S., Sengupta, R., Chakraborty, M. (1997). Elemental Chemistry of Ilmenite - An Indicator of Provenance? *Journal of the Geological Society of India* 50, pp. 787–789. https://doi.org/10.17491/JGSI/1997/500616

Biró, T., Hencz, M., Németh, K., Karátson, D., Márton, E., Szakács, A., Bradák, B., Szalai, Z., Pécskay, Z., Kovács, I.J. (2020). A Miocene Phreatoplinian eruption in the North-Eastern Pannonian Basin, Hungary: The Jató Member. *Journal of Volcanology and Geothermal Research* 401, p.106973. https://doi.org/10.1016/J.JVOLGEORES.2020.106973

Biró, T., Hencz, M., Telbisz, T., Cseri, Z., Karátson, D. (2022). The relationship between ignimbrite lithofacies and topography in a foothill setting formed on Miocene pyroclastics – a case study from the Bükkalja, Northern Hungary. *Hungarian Geographical Bulletin* 71, pp. 213–229. https://doi.org/10.15201/HUNGEOBULL.71.3.1

Bowles, J.F.W., Howie, R.A., Vaughan, D.J., Zussman, J. (2011). Non-silicates: volume 5A. Rock-forming minerals 920.

Csontos, L., Nagymarosy, A., Horváth, F., Kovác, M. (1992). Tertiary evolution of the Intra-Carpathian area: A model. *Tectonophysics* 208, pp. 221–241. https://doi.org/10.1016/0040-1951(92)90346-8

Czuppon, G., Lukács, R., Harangi, S., Mason, P.R.D., Ntaflos, T. (2012). Mixing of crystal mushes and melts in the genesis of the Bogács Ignimbrite suite, northern Hungary: An integrated geochemical investigation of mineral phases and glasses. *Lithos* 148, pp. 71–85. https://doi.org/10.1016/J.LITHOS.2012.06.009

Downs, R.T., Hall-Wallace, M. (2003). The American Mineralogist crystal structure database. *American Mineralogist* 88, pp. 247–250.

Ganzha, O., Okholina, T., Kroshko, Y., Kuzmanenko, H., Kovalchuk, M. (2023). Structural and Lithological Models of Ilmenite Placer Deposits in Ukraine. *Anuario do Instituto de Geociencias* 46. https://doi.org/10.11137/1982-3908_2023_46_55949

Harangi, S., Mason, P.R.D., Lukács, R. (2005). Correlation and petrogenesis of silicic pyroclastic rocks in the Northern Pannonian Basin, Eastern-Central Europe: In situ trace element data of glass shards and mineral chemical

constraints. *Journal of Volcanology and Geothermal Research* 143, pp. 237–257. https://doi.org/10.1016/J.JVOLGEORES.2004.11.012

Hencz, M., Biró, T., Németh, K., Szakács, A., Portnyagin, M., Cseri, Z., Pécskay, Z., Szabó, C., Müller, S., Karátson, D. (2024). Lithostratigraphy of the ignimbrite-dominated Miocene Bükk Foreland Volcanic Area (Central Europe). *Journal of Volcanology and Geothermal Research* 445, p. 107960. https://doi.org/10.1016/j.jvolgeores.2023.107960

Herz, N., Valentine, L.E., Iberall, E.R., Hickel, W.J., Pecora, W.T. (1970). Rutile and ilmenite placer deposits, Roseland district, Nelson and Amherst Counties, Virginia. *Bulletin*. https://doi.org/10.3133/B1312F

Kolb, J., Keiding, J.K., Steenfelt, A., Secher, K., Keulen, N., Rosa, D., Stensgaard, B.M. (2016). Metallogeny of Greenland. *Ore Geol Rev* 78, pp. 493–555. https://doi.org/10.1016/J.OREGEOREV.2016.03.006

Kovács, I., Szabó, C. (2008). Middle Miocene volcanism in the vicinity of the Middle Hungarian zone: Evidence for an inherited enriched mantle source. J *Geodyn* 45, pp. 1–17. https://doi.org/10.1016/j.jog.2007.06.002

Lattard, D. (1995). Experimental evidence for the exsolution of ilmenite from titaniferous spinel. *American Mineralogist* 80, pp. 968–981. https://doi.org/10.2138/AM-1995-9-1013

Lukács, R., Harangi, S., Gál, P., Szepesi, J., Di Capua, A., Norini, G., Sulpizio, R., Groppelli, G., Fodor, L. (2022). Formal definition and description of lithostratigraphic units related to the Miocene silicic pyroclastic rocks outcropping in Northern Hungary: A revision. *Geologica Carpathica* 73, pp. 137–158. https://doi.org/10.31577/GeolCarp.73.2.3

Lukács, R., Harangi, S., Guillong, M., Bachmann, O., Fodor, L., Buret, Y., Dunkl, I., Sliwinski, J., von Quadt, A., Peytcheva, I., Zimmerer, M. (2018). Early to Mid-Miocene syn-extensional massive silicic volcanism in the Pannonian Basin (East-Central Europe): Eruption chronology, correlation potential and geodynamic implications. *Earth Sci Rev* 179, pp. 1–19. https://doi.org/10.1016/J.EARSCIREV.2018.02.005

MacDonald, W.G., Rozendaal, A. (1995). The Geelwal Karoo heavy mineral deposit: a modern day beach placer. *Journal of African Earth Sciences* 21, pp. 187–200. https://doi.org/10.1016/0899-5362(95)00082-5

Mücke, A., Bhadra Chaudhuri, J.N. (1991). The continuous alteration of ilmenite through pseudorutile to leucoxene. *Ore Geol Rev* 6, pp. 25–44. https://doi.org/10.1016/0169-1368(91)90030-B

Murphy, P., Frick, L. (2006). Titanium, in: Barker, J.M., Kogel, J.E., Trivedi, N.C., Krukowski, S.T. (Eds.), Industrial Minerals & Rocks : Commodities, Markets,

and Uses. *Society for Mining, Metallurgy, and Exploration*, Littleton, Colorado, pp. 990–991.

Nayak, B., Mohanty, S., Bhattacharyya, P. (2012). Heavy Minerals and the Characters of Ilmenite in the Beach Placer Sands of Chavakkad-Ponnani, Kerala Coast, India. *Journal of the Geological Society of India* 79, pp. 259–266. https://doi.org/10.1007/S12594-012-0046-7

Prates Hallal, G., Porcher, C.C., Veettil, B.K., De Almeida Espinoza, J.M., Beatriz Alves Rolim, S. (2025). Distribution of ilmenite minerals in placer deposits along the middle coast of Southern Brazil using spaceborne and ground-based remote sensing. *PLoS One* 20, e0314238. https://doi.org/10.1371/JOURNAL.PONE.0314238

Rahman, A., Tardio, J., Bhargava, S.K., Zaman, M.N., Hasan, A.S.M.M., Torpy, A., Pownceby, M.I. (2020). Comparison of the chemistry and mineralogy of ilmenite concentrates sourced from fluvial (Brahmaputra River) and beach placer (Cox's Bazar) deposits, Bangladesh. *Ore Geol Rev* 117, p. 103271. https://doi.org/10.1016/J.OREGEOREV.2019.103271

Ramakrishnan, C., Mani, R., Babu, D.S.S. (1997). Ilmenite from the Chavara deposit, India: a critical evaluation. *Mineral Mag* 61, pp. 233–242. https://doi.org/10.1180/MINMAG.1997.061.405.06

Roy, P.S. (1999). Heavy mineral beach placers in southeastern Australia; their nature and genesis. *Economic Geology* 94, pp. 567–588. https://doi.org/10.2113/GSECONGEO.94.4.567

Rudnick, R., Gao, S. (2013). Composition of the Continental Crust. *Treatise on geochemistry* 4. https://doi.org/10.1016/B978-0-08-095975-7.00301-6

Schipper, C., Rickard, W., Reddy, S., Saxey, D., Castro, J., Fougerouse, D., Quadir, M., Conway, C., Prior, D., Lilly, K. (2020). Volcanic SiO2-cristobalite: A natural product of chemical vapor deposition. *American Mineralogist* 105, pp. 510–524. https://doi.org/10.2138/am-2020-7236

Szakács, A., Márton, E., Póka, T., Zelenka, T., Pécskay, Z., Seghedi, I. (1998). Miocene acidic explosive volcanism in the Bukk Foreland, Hungary: Identifying eruptive sequences and searching for source locations. *Acta Geologica Hungarica* 41, pp. 413–435.

Szakáll, S., Kristály, F. (2021). Cassiterite in quartz-feldspar veinlets of ignimbrite (Southern Bükk Mts., Hungary). *Acta Mineralogica Petrographica Abstract Series* 11, p. 42.

Wassef, S.N. (1981). Distribution and properties of placer ilmenite in East Rosetta beach sands, Egypt. *Miner Depos* 16, pp. 259–267. https://doi.org/10.1007/BF00202739/METRICS

Wells, H.C., Haverkamp, R.G. (2020). Characterization of the Heavy Mineral Suite in a Holocene Beach Placer, Barrytown, New Zealand. *Minerals* 2020, Vol. 10, p. 86 https://doi.org/10.3390/MIN10020086